Available online at www.sciencedirect.com
ScienceDirect
Journal of Solid State Chemistry 181 (2008) 382–391
JOURNAL OF SOLID STATE CHEMISTRY
www.elsevier.com/locate/jssc

Hydrothermal syntheses, structural, Raman, and luminescence studies of $Cm[M(CN)_2]_3 \cdot 3H_2O$ and $Pr[M(CN)_2]_3 \cdot 3H_2O$ (M = Ag, Au) 2. Hetero-bimetallic coordination polymers consisting of trans-plutonium and transition metal elements

Zerihun Assefa[a,*], Richard G. Haire[b], Richard E. Sykora[c]

[a]*Department of Chemistry, North Carolina A&T State University, Greensboro, NC 27411, USA*
[b]*Chemical Sciences Division, Oak Ridge National Laboratory, Oak Ridge, TN 37831, USA*
[c]*Department of Chemistry, University of South Alabama, Mobile, AL 36688, USA*

Received 22 September 2007; received in revised form 22 November 2007; accepted 26 November 2007
Available online 18 January 2008

Abstract

We have prepared $Cm[Au(CN)_2]_3 \cdot 3H_2O$ and $Cm[Ag(CN)_2]_3 \cdot 3H_2O$ as a part of our continuing investigations into the chemistry of the 5*f*-elements' dicyanometallates. Single crystals of $Cm[Au(CN)_2]_3 \cdot 3H_2O$ were obtained from the reaction of $CmCl_3$ and $KAu(CN)_2$ under mild hydrothermal conditions. Due to similarities in size, the related praseodymium compounds were also synthesized and characterized for comparison with the actinide systems. The compounds crystallize in the hexagonal space group $P6_3/mcm$, where the curium and the transition metals interconnect through cyanide bridging. Crystallographic data (Mo Kα, $\lambda = 0.71073$ Å): $Cm[Au(CN)_2]_3 \cdot 3H_2O$ (**1**), $a = 6.6614(5)$ Å, $c = 18.3135(13)$ Å, $V = 703.77(9)$, $Z = 2$; $Pr[Au(CN)_2]_3 \cdot 3H_2O$ (**3**), $a = 6.6662(8)$ Å, $c = 18.497(3)$ Å, $V = 711.83(17)$, $Z = 2$; $Pr[Ag(CN)_2]_3 \cdot 3H_2O$ (**4**), $a = 6.7186(8)$ Å, $c = 18.678(2)$ Å, $V = 730.18(14)$, $Z = 2$. The Cm^{3+} and/or Pr^{3+} ions are coordinated to six N-bound CN^- groups resulting in a trigonal prismatic arrangement. Three oxygen atoms of coordinated water molecules tricap the trigonal prismatic arrangement providing a coordination number of nine for the *f*-elements. The curium ions in both compounds exhibit a strong red emission corresponding to the $^6D_{7/2} \rightarrow {}^8S_{7/2}$ transition. This transition is observed at 16,780 cm^{-1}, with shoulders at 17,080 and 16,840 cm^{-1} for the Ag complex, while the emission is red shifted by ~100 cm^{-1} in the corresponding gold complex. The Pr systems also provide well-resolved emissions upon *f–f* excitation.

Keywords: Trans-plutonium complexes; Coordination polymer; Emission; Hydrothermal syntheses

1. Introduction

The importance of metal containing polymers for new materials is quite extensive and Au(I), Ag(I), and Pt(II) based polymers are of particular importance due to their unique photophysical properties [1,2]. In this regard, cyanide-bridged bimetallic systems, prepared by assembling cyanometallates and transition metal and/or lanthanide building blocks exhibit fascinating structural, magnetic, electrochemical, and magneto-optical properties [3–5]. Metal-cyanide anions have played a prominent role in the design of supramolecular coordination polymers [6,7] as they readily form strong bonds with transition metal cations and are excellent mediators of electronic and magnetic exchange. This has been demonstrated by their ubiquitous use in the synthesis of prussian-blue type, high-*T*c molecule-based magnets [4].

The simple and linear dicyanoaurate $[Au(CN)_2]^-$ anion, has been extensively studied as a building block to form coordination polymers through cyanide bridging. It can form polymers in a fashion similar to other metal-cyanide anions, but is unique in that its central Au(I) atom is prone to forming gold–gold bonds both in solution [8,9] and in the solid state [10–13]. The "aurophilic" interactions are now widely accepted as a prominent example of a more

*Corresponding author. Fax: +1 336 334 7124.
E-mail address: zassefa@ncat.edu (Z. Assefa).

0022-4596/$ - see front matter © 2008 Elsevier Inc. All rights reserved.
doi:10.1016/j.jssc.2007.11.036

general phenomenon of metallophilicity, and recognized as a major force determining supramolecular structures and properties [14,15]. Although many homometallic Au(I) polymers formed by virtue of these "aurophilic" interactions have been studied [16], heterometallic polymers incorporating such gold–gold interactions are less common.

A class of coordination compounds that have been investigated widely include the lanthanide dicyanoaurates [8,9,15] and to a lesser degree, their dicyanoargentate counterparts [12,17]. Examples of coordination polymers involving trans-plutonium elements, however, have been reported just recently for $Am[M(CN)_2]_3 \cdot 3H_2O$ (M = Ag, Au) [18], with an earlier example of a trans-uranium coordination polymer having been reported for a neptunium chromate system [19]. Although the chemistry of 5*f* actinide(III) compounds are expected to parallel that of the 4*f*-lanthanides, the understanding of the subtle differences in the structural features of compounds containing these two series of elements is limited, mainly because of the challenge and restrictions associated with handling the intensely radioactive 5*f*-element compounds. The high radio toxicity of the materials and safety protocols that needed also restrict the experimental procedures that can be adapted. Hence, single-crystal structural studies of the trans-plutonium compounds are rare. As a result, most of the compounds are structurally unexplored due to the special equipment and facilities needed to study them. Crystal deterioration due to self-irradiation poses an additional challenge.

We have recently reported on $Am[Au(CN)_2]_3 \cdot 3H_2O$ and $Am[Ag(CN)_2]_3 \cdot 3H_2O$ which also represent two examples of a trans-plutonium element bonded to a transition metal through cyanide bridging to form a three-dimensional coordination polymeric structure [18]. Continuing with this effort the structural and spectroscopic properties of the polymeric compounds between the man-made element, curium, and gold and silver dicyanides, $Cm[Au(CN)_2]_3 \cdot 3H_2O$ and $Cm[Ag(CN)_2]_3 \cdot 3H_2O$, are reported here.

The preparation technique employed for their syntheses was the less-conventional hydrothermal procedure. When compared to the more traditional, slow-evaporation technique, the hydrothermal synthetic procedure was especially favorable for fast single crystal growth needed to counter high radioactivity induced crystal deterioration from within. The praseodymium systems are used for structural and spectroscopic comparisons, since Pr^{3+} has a similar ionic size to that of Cm^{3+}.

2. Experimental section

2.1. Materials and methods

The ^{248}Cm isotope used in these studies was made available by the US Department of Energy. $PrCl_3 \cdot xH_2O$ (Alfa-Aesar; 99.9%), $KAg(CN)_2$ (Alfa-Aesar; 99.9%), and $KAu(CN)_2$ (Alfa-Aesar; 99.99%) were used as received. Triply distilled water was used in all reactions. An aqueous $CmCl_3$ solution was prepared by dissolving $CmCl_3$ in 0.1 M HCl. Manipulations necessary to prepare $Cm[M(CN)_2]_3 \cdot 3H_2O$ (M = Ag, Au) were conducted in glove boxes in accordance with the established policies for handling radioactive materials at the Oak Ridge National Laboratory. To decrease the likelihood of radioactive contamination, samples selected for X-ray and spectroscopic analyses were doubly contained. *It should be noted that special training and experimental facilities are required in order to perform work with highly radioactive trans-uranium materials, such as curium.*

2.2. Syntheses of $Cm[M(CN)_2]_3 \cdot 3H_2O$ (M = Au, (**1**); Ag, (**2**))

The synthesis of compound **1** was accomplished by adding aqueous $CmCl_3$ (35 μL, 0.12 M) to a quartz reaction vessel that had been loaded with solid $KAu(CN)_2$ (3.89 mg, 13.5 μmol). The reaction vessel was sealed, placed in a furnace, and then heated to 120 °C, where the reaction/crystallization occurred under autogenously generated pressure. After 68 h, the furnace was turned off and allowed to self-cool to room temperature. Single crystals of **1** were obtained from the reaction. The crystals had a reddish brown coloration and were in the shape of hexagonal plates. The synthesis of **2** was similar to that of **1**, except that $KAg(CN)_2$ was used in place of the $KAu(CN)_2$. However, this reaction did not provide single crystals suitable for X-ray crystallographic studies.

2.3. Syntheses of $Pr[M(CN)_2]_3 \cdot 3H_2O$ (M = Au, (**3**); Ag, (**4**))

The syntheses of compounds **3** and **4** were performed in a manner similar to that described above for the curium compounds. For compound **3** aqueous $PrCl_3$ (108.9 μL, 0.196 M) and $KAu(CN)_2$ (18.44 mg, 64.01 μmol) were reacted, while aqueous $PrCl_3$ (106.5 μL, 0.196 M) and $KAg(CN)_2$ (12.46 mg, 62.60 μmol) were used in the synthesis of **4**. Crystals of **3** and **4** have been isolated in the form of hexagonal plates, hexagonal needles, and irregularly shaped prisms. All of these compounds were confirmed to be isostructural by X-ray diffraction methods. The average yields for **3** and **4** are 60% based on multiple syntheses.

2.4. Single-crystal X-ray diffraction

Intensity data were collected from **1** with the use of a Bruker SMART APEX CCD X-ray diffractometer. The crystal of **1** was sealed in a quartz capillary and then placed inside of a polyethylene tube for secondary containment. Intensity data for **3** and **4** were collected on an Enraf-Nonius CAD-4 X-ray diffractometer from single crystals mounted on the tips of quartz fibers. Intensity measurements for all compounds were performed using graphite

Table 1
Crystallographic data for $Cm[Au(CN)_2]_3 \cdot 3H_2O$ (**1**), $Pr[Au(CN)_2]_3 \cdot 3H_2O$ (**3**), and $Pr[Ag(CN)_2]_3 \cdot 3H_2O$ (**4**)

Formula	$Cm[Au(CN)_2]_3 \cdot 3H_2O$	$Pr[Au(CN)_2]_3 \cdot 3H_2O$	$Pr[Ag(CN)_2]_3 \cdot 3H_2O$
Formula mass	1049.14	941.98	674.69
Crystal system	Hexagonal	Hexagonal	Hexagonal
Space group	$P6_3/mcm$ (no. 193)	$P6_3/mcm$ (no. 193)	$P6_3/mcm$ (no. 193)
a (Å)	6.6614(5)	6.6662(8)	6.7186(8)
c (Å)	18.3135(13)	18.497(3)	18.678(2)
V (Å^3)	703.77(9)	711.83(17)	730.18(14)
Z	2	2	2
T (K)	290	290	290
λ (Å)	0.71073	0.71073	0.71073
$2\theta_{max}$	56.56	50.70	50.74
ρ_{calcd} (g cm^{-3})	4.951	4.395	3.069
μ(Mo Kα) (mm^{-1})	36.912	34.190	7.250
Reflections collected	6314	875	900
Independent reflections	349 [$R_{int} = 0.0480$]	263 [$R_{int} = 0.0528$]	272 [$R_{int} = 0.0467$]
Data/restraints/parameters	349/0/24	263/0/24	272/0/24
$R(F)$[a] for $F_o^2 > 2\sigma(F_o^2)$ [a]	0.0174	0.0308	0.0303
$R_w(F_o^2)$ [b]	0.0391	0.0814	0.0738

[a] $R(F) = \sum ||F_o| - |F_c|| / \sum |F_o|$.

[b] $R_w(F_o^2) = \left[\sum w(F_o^2 - F_c^2)^2 / \sum wF_o^4\right]^{1/2}$.

monochromated, Mo Kα radiation from a sealed X-ray tube.

For **1**, the determination of integrated intensities and a global cell refinement were performed with the Bruker SAINT (version 6.02) software package using a narrow-frame, integration algorithm. A semi-empirical absorption correction was applied using SADABS [20]. XCAD4 [21] was used to process the data collected on the CAD-4. For all three data sets, the program suite SHELXTL (version 5.1) was used for space group determination (XPREP), structure solution (XS), and least-squares refinement (XL) [22]. A Patterson function was used to locate the metal atom positions. The C, N, and O atomic positions were located in difference maps. The hydrogen atoms of the water molecules were not located or calculated. The scattering factor, real and imaginary dispersion terms, and the linear absorption coefficient for curium [23] were manually inserted into the SHELXTL instruction file. The final refinements for all compounds included anisotropic displacement parameters for all atoms and a secondary extinction parameter was included for **1** and **3**. Some crystallographic details for compounds **1**, **3**, and **4** are listed in Table 1. Further details of the crystal structure investigations may be obtained from the Fachinformationzentrum Karlsruhe, 76344 Eggenstein-Leopoldshafen, Germany (e-mail: crysdata@fiz-karlsruhe.de; http://www.fiz-karlsruhe.de/request_for_deposited_data.html; fax: (+49)7247-808-666) on quoting the depository numbers CSD-418552 for **1**, CSD-418553 for **3**, and CSD-418554 for **4**.

2.5. Raman spectroscopy

Raman spectroscopy experiments were performed using an argon-ion laser (Coherent; model 306) and a double-meter spectrometer (Jobin-Yvon Ramanor model HG.2S). As a double-meter spectrometer, the Ramanor has a total of four slits (one entrance, one exit and two internal slits) that are manually controlled. Based on the manufacturer's calibration, the maximum resolution for the monochromator at 514.5 nm is 0.5 cm^{-1}. However, the resolution for the spectra reported here varied from sample to sample. The actual resolution of the Raman signal for the samples varied between 1 and 2 cm^{-1}. Most of the spectra were collected at a dwell time of 0.5 s/pt, and the signal detection was acquired using a water-cooled photo-multiplier tube (Hamamatsu R636). The analog signal from the PMT was digitized using an ADC interfaced with the instrument and the data was subsequently stored in a personal computer. The LabSpec (version 3.04) software controlled scanning and other instrumental functions. The curium samples in sealed capillary tubes, were then inserted into secondary glass tubes to provide double containment.

2.6. Photoluminescence studies

The 457.8 nm argon ion laser line was used for excitation of the curium complexes. The high resolution spectra of the praseodymium complexes were also obtained by exciting with the 457.8 nm argon laser line, whereas the low resolution spectra were collected using 360 nm excitation from a Xe-lamp. The luminescence spectra were collected using an Instrument SA optical system consisting of a monochromator (model 1000 M) attached to CCD, PMT, and IR detectors. Additional higher resolution spectra were collected using a HG2.S monochromator. Data analyses were performed with Grams/32 software (Galactic, version 5.1). Additional luminescence work was conducted on the Pr systems (compounds **3** and **4**) at NCAT State University using a photon technology international (PTI) spectrometer (model QM-7/SE). The system has a high-intensity

Table 2
Selected bond distances (Å) for $Cm[Au(CN)_2]_3 \cdot 3H_2O$ (**1**), $Pr[Au(CN)_2]_3 \cdot 3H_2O$ (**3**), and $Pr[Ag(CN)_2]_3 \cdot 3H_2O$ (**4**)

$Cm[Au(CN)_2]_3 \cdot 3H_2O$		$Pr[Au(CN)_2]_3 \cdot 3H_2O$		$Pr[Ag(CN)_2]_3 \cdot 3H_2O$	
Cm(1)–N(1)	2.570(9)	Pr(1)–N(1)	2.607(12)	Pr(1)–N(1)	2.600(3)
Cm(1)–O(1)	2.454(12)	Pr(1)–O(1)	2.497(15)	Pr(1)–O(1)	2.485(4)
Au(1)–C(1)	1.997(9)	Au(1)–C(1)	1.975(13)	Ag(1)–C(1)	2.057(3)
C(1)–N(1)	1.134(14)	C(1)–N(1)	1.163(18)	C(1)–N(1)	1.138(4)
Au(1)···Au(1)′	3.3307(2)	Au(1)···Au(1)′	3.3331(4)	Ag(1)···Ag(1)′	3.3593(4)

xenon source for excitation. Wavelength selection for excitation and emission is conducted by means of computer controlled, autocalibrated "QuadraScopic" monochromators which are equipped with aberration corrected emission and excitation optics. For the low-temperature work, the sample was in a sealed capillary tube inserted in a cold-finger dewar filled with liquid nitrogen. For signal detection a PMT detector (model 928) that can work either in analog or digital (photon counting) modes was used. Emission spectra are corrected by a factory correction methodology. Instrument operation, data collection, and handling were all controlled using advanced FeliX32 fluorescence spectroscopic package.

3. Results and discussion

3.1. Synthesis of materials

Multiple techniques have been reported to prepare bimetallic cyanide coordination polymers containing transition metal and lanthanide or actinide ions. For example, the syntheses of $Eu[Ag(CN)_2]_3 \cdot 3H_2O$ [12], $Eu[Au(CN)_2]_3 \cdot 3H_2O$ [15], and $Tb[Au(CN)_2]_3 \cdot 3H_2O$ [13] have all been reported using the slow evaporation technique. Colis et al. reported crystal growth of several $La[Ag_xAu_{1-x}(CN)_2]_3 \cdot 3H_2O$ compounds in agar gels [24,25]. As described in the experimental section, the syntheses of compounds **1**–**4** were accomplished using a hydrothermal technique. A more detailed explanation of the method has been published elsewhere for the $Am[M(CN)_2]_3 \cdot 3H_2O$ system [18]. The synthetic procedure has also been used recently in the preparation of other mixed metal cyanide complexes [26,27]. The hydrothermal method is particularly attractive for the synthesis of the actinide dicyanometallate compounds, due to the fact that single crystals can be grown rapidly with small quantities of reactants (<1 mg).

3.2. Description of the crystal structures

The three new compounds whose structures are reported here all contain the $Eu[Ag(CN)_2]_3 \cdot 3H_2O$ structure type [12]. Compounds in this class crystallize in the hexagonal space group, $P6_3/mcm$. This structure type has also recently been reported for two trans-plutonium compounds $Am[Ag(CN)_2]_3 \cdot 3H_2O$ and $Am[Au(CN)_2]_3 \cdot 3H_2O$ [18] and a number of lanthanide compounds in this class have also been described [10–13]. Detailed reports describing the structure have been published [12,24,25,29]. Due to the structural similarities of the compounds reported here, only a brief description of **1** will be given. Table 1 contains the crystallographic data for compounds **1**, **3**, and **4**. Lists of selected bond lengths and angles for the compounds are given in Table 2. Atomic coordinates and equivalent isotropic displacement parameters for **1** are given in Table 3.

Table 3
Atomic coordinates and equivalent isotropic displacement parameters for $Cm[Au(CN)_2]_3 \cdot 3H_2O$

Atom (site)	x	y	z	U_{eq} (Å^2)[a]
Cm(1)	1	0	1/4	0.008(1)
Au(1)	1/2	0	0	0.019(1)
C(1)	0.6491(16)	0	0.0946(5)	0.018(2)
N(1)	0.7349(14)	0	0.1481(5)	0.024(2)
O(1)	1.3683(18)	0	1/4	0.039(3)

[a] U_{eq} is defined as one-third of the trace of the orthogonalized U_{ij} tensor.

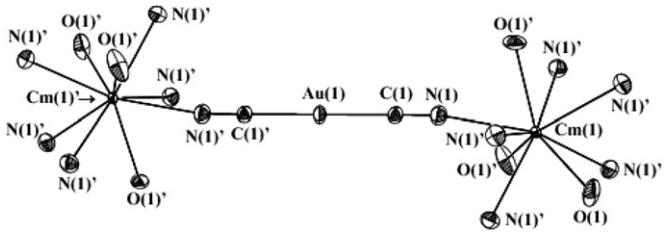

Fig. 1. An illustration of the tricapped trigonal prismatic environment around the Cm^{3+} ions in $Cm[Au(CN)_2]_3 \cdot 3H_2O$. Fifty percent displacement ellipsoids are shown.

Fig. 1 shows the coordination geometry around the curium atom with the atomic labeling scheme included. The Cm^{3+} ion has a tricapped trigonal prismatic coordination geometry with a D_{3h} site symmetry. The three O atoms of the water molecules are coplanar with the Cm atom, by symmetry. The six nitrogen atoms in the inner sphere of the Cm^{3+} ion are also related by symmetry. In the structure, the Cm and Au atoms are found in alternating parallel layers (crystallographic *ab* planes) as shown in Fig. 2. These alternating layers of Au and Cm atoms are bridged with cyanide linkages resulting in an overall three-dimensional framework. Every Au atom has four nearest

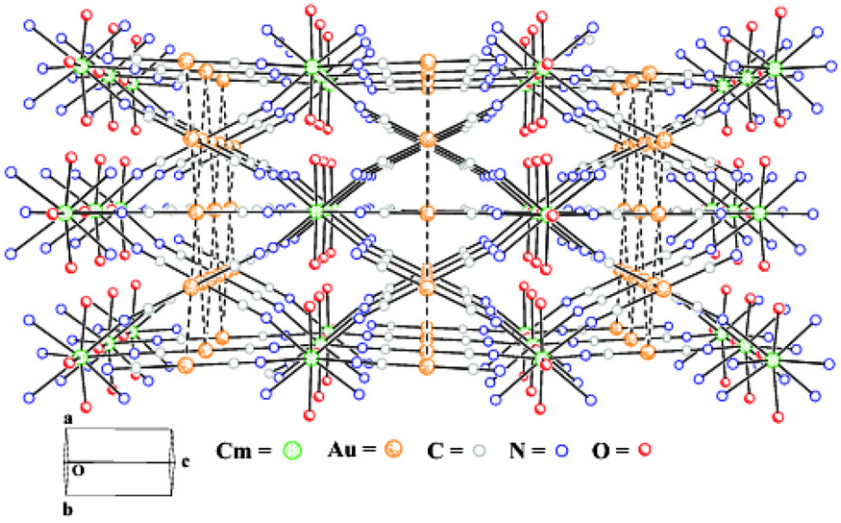

Fig. 2. The packing diagram for $Cm[Au(CN)_2]_3 \cdot 3H_2O$ viewed parallel to the *ab* plane.

neighbors forming a Kagomé network; the Au···Au distances in these layers are 3.3307(2) Å. The one crystallographic gold atom is coordinated to the carbon atoms of two bridging cyanide ligands, resulting in nearly linear $Au(CN)_2^-$ units as found in other dicyanometallates [18,28,29].

Very few literature values are available for comparison of Cm–O and/or Cm–N bond distances due to the limited number of diffraction [30–36] or scattering experiments [34] on Cm-containing compounds. The Cm–O distance of 2.454(12) Å in **1** is shorter than the Cm–N distance of 2.570(9) Å. The Cm–O bond length is comparable to that found for the coordinated water molecules in $[Cm(H_2O)_9](CF_3SO_3)_3$ [34] (2.453(1) and 2.545(1)). A similar Cm–O bond distance in both compounds is expected since the hydrated Cm^{3+} ion in the structure of $[Cm(H_2O)_9](CF_3SO_3)_3$ is nine-coordinate and also contains a tri-capped trigonal prismatic geometry. The only Cm–N distance found in the literature is in the ionic compound CmN [30], the Cm–N distance is 2.514 Å.

A trend observed in this class of compounds is that for a particular lanthanide or actinide metal the overall structural features remain unchanged when gold is replaced by silver [18,24,27–29]. However, the Au···Au separations are generally slightly smaller than the Ag···Ag separations in related compounds containing the same *f*-element. For example, the Au···Au distance in **3** is 3.3331(4), while the Ag···Ag distance in **4** is 3.3593(4). Similar trends have been noticed in the Am [18], Nd [18], and Tb [29] systems as well. Consistent with the general trend observed so far, the unit cell volume in **3** is smaller by ~2.7% as compared with the silver analog (see Table 1). Although gold is heavier than silver, the reduction in volume is traced to the smaller covalent radii caused by the larger "relativistic contraction" in gold [37–39]. The bonding interactions with gold reflect that it is more prone for covalent interaction than silver [39].

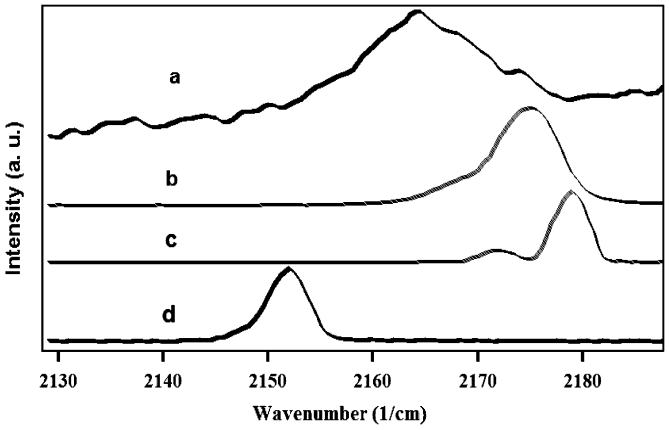

Fig. 3. Raman spectra of: (a) $Cm[Ag(CN)_2]_3 \cdot 3H_2O$, (b) $Pr[Au(CN)_2]_3 \cdot 3H_2O$ (room temperature), (c) $Pr[Au(CN)_2]_3 \cdot 3H_2O$ (liquid N_2 temperature), and (d) $Pr[Ag(CN)_2]_3 \cdot 3H_2O$ (liquid N_2 temperature) in the ν_{CN} stretching region.

3.3. Raman spectroscopy

The Raman spectra of the complexes covering the ν_{CN} stretching region are shown in Fig. 3. The ν_{CN} symmetric stretch for $KAg(CN)_2$ at 2145 cm^{-1} [18] blue shifts by ~18 cm^{-1} upon coordination with Cm and appears at 2163 cm^{-1} (Fig. 3(a)). It is important to note that due to the small size of the sample of compound **2**, a large number of data points were required to average out the noise, although a similar effort with compound **1** did not provide a quality spectrum. The blue-shift in the ν_{CN} stretch indicates bridging of the two metals (Cm and Ag) resulting in a substantial electron density removal from the cyanide group. The Raman profile for the Pr^{3+} system is shown in Fig. 3(b)–(d). The spectrum of compound **3** in Fig. 3(b) consists of a broad band at 2175 cm^{-1} (FWHM = 7.2 cm^{-1}) and a shoulder at 2169 cm^{-1}. The band sharpens at liquid N_2 temperature, and is observed at 2177 cm^{-1}

(FWHM = 4 cm^{-1}). The shoulder also becomes a well-defined band and appears at 2170 cm^{-1}. For compound **4** (Fig. 3(d)), the ν_{CN} symmetric stretch is observed is significantly red-shifted to 2153 cm^{-1} when compared with the gold system.

Accumulated literature data indicates that the ν_{CN} frequencies appear at higher energies in all of the gold dicyanide complexes, when compared with their silver analogs [15,24,25]. The shift to higher frequency is consistent with the structural data where the carbon–nitrogen bond distances are shorter in the gold-compounds. Nevertheless, the ν_{CN} symmetric stretch blue shifts in both **3** and **4** when compared with those found in the starting compounds. The blue-shift in the ν_{CN} stretch indicates bridging of the two metals (gold and praseodymium), resulting in a substantial electron density removal from the cyanide group. The shift to higher energy of the ν_{CN} is consistent with data reported for most cyanometalates that show blue-shifting upon nitrile [15,40,41] binding. This blue-shift is rationalized in terms of a substantial electron density withdrawal from the anti-bonding N lone pair upon bridging with *f*-ions. Only metals such as Tl and Pb, which participate in back-bonding to the CN group, are known to exhibit red-shifted ν_{CN} symmetric stretching bands [42].

In Fig. 4, the Raman profile of the praseodymium system is provided in the low energy region. Although not clearly defined in the $KAg(CN)_2$ spectrum [18], compound **4** has a well-resolved doublet (Fig. 4(a)) at 400 and 369 cm^{-1}, which is assignable to the ν_{Ag-C} stretch. A broad band centered at 268 cm^{-1} is also observed with a shoulder at 254 cm^{-1}. This band is blue shifted, significantly compared with that for $KAg(CN)_2$ [18], which is observed at 249 cm^{-1}. The bands are assignable to the Ag–C–N bending modes.

The ν_{Au-C} stretching in compound **3** appears as a doublet (Fig. 4(b)) at blue-shifted positions of 487 and 470 cm^{-1} compared with the silver analogs. The blue-shift is consistent with a stronger Au–C bond inferred from the *M*–C distances (1.975 vs. 2.057 Å in Au–C vs. Ag–C, respectively). The Au–C–N bending mode in **3** is also blue-shifted to 342 and 326 cm^{-1} when compared with the values for the Ag–C–N modes (Fig. 4(a)), and the Au–C–N bending in $KAu(CN)_2$ [18]. Additional Raman bands are also observed in the lower energy region at 223, 174, 145, and 111 cm^{-1}. All of these bands are assignable to lattice modes. Following a prior assignment [43], the broad band centered at 78 cm^{-1} is assigned to the Au–Au symmetric stretching.

Although, it would be desirable to compare the lanthanide data with that of the actinide complexes, the size of the sample available for the Raman analysis combined with the reduced signal intensity in the low-frequency vibrational region limited our ability to collect meaningful data on the curium compounds. However, the structural comparison indicates that the Au–C distance in **1** is longer than that of **3** and, thus, a red-shift is anticipated in the ν_{Au-C} vibrational modes of the actinide compounds as compared to the Pr-systems. The same trend has been observed in other similar structures [18].

3.4. Photoluminescence studies

3.4.1. $Cm[M(CN)_2]_3 \cdot 3H_2O$ (M = Au, Ag)

The photoluminescence spectra of compounds **1** and **2** are shown in Fig. 5(a) and (b). The emission spectrum of the Au compound was collected on single crystals. As shown in Fig. 5(b), the strongest peak is observed at 16,780 cm^{-1} with distinct shoulders at the high-energy side of the spectrum at 17,080 and 16,840 cm^{-1} providing a total splitting of about 300 cm^{-1} between the highest and lowest peaks. Based on the *f*-level structure of Cm^{3+}, the emission originates from the first excited $J = 7/2$ state. The ground state, $^8S_{7/2}$, of the half-filled $5f^7$ configuration of Cm^{3+} is spherically symmetric and, thus, only a small splitting (few wavenumbers) is expected due to inner sphere coordinating ligands. Hence, the total splitting of ~300 cm^{-1} observed in the emission spectrum cannot be assigned to ground state splitting, and is attributable to ligand field splitting of the excited $J = 7/2$ level where the emission originates. The most intense emission band at 16,780 cm^{-1} is assigned as originating from the lowest Stark level of the $J = 7/2$ ($^6D_{7/2}$) excited state, while the higher-energy splittings are assigned to the higher Stark

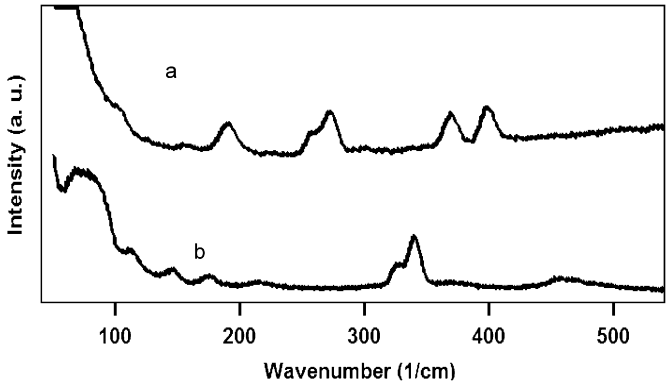

Fig. 4. Raman spectra of: (a) $Pr[Ag(CN)_2]_3 \cdot 3H_2O$ and (b) $Pr[Au(CN)_2]_3 \cdot 3H_2O$ in the low-frequency region.

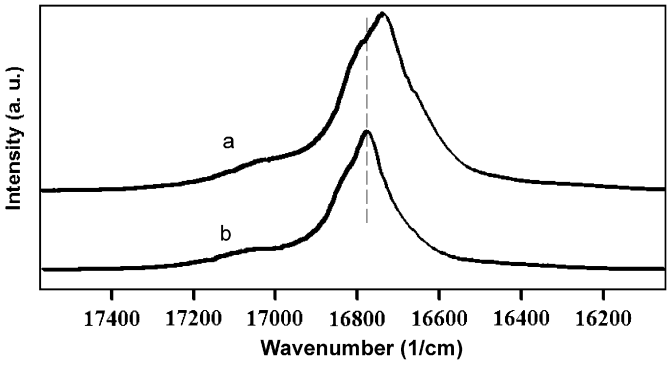

Fig. 5. Emission Spectra of: (a) $Cm[Au(CN)_2]_3 \cdot 3H_2O$ and (b) $Cm[Ag(CN)_2]_3 \cdot 3H_2O$.

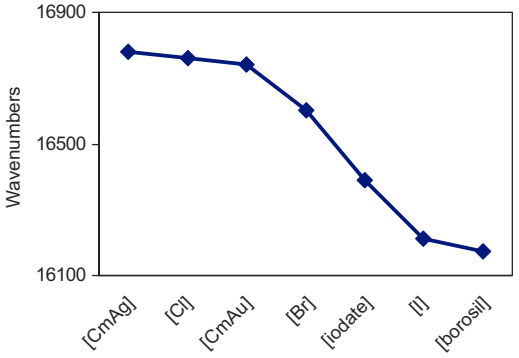

Fig. 6. Dependence of the emission energy of the Cm^{3+} *f–f* transition on coordination environment. Curium halides are represented by [Cl], [Br], [I]; curium iodate is represented by [iodate]; [borosil], corresponds to data of curium doped in borosilcate silicate glass. [CmAu] and [CmAg] correspond to compounds **1** and **2**, respectively.

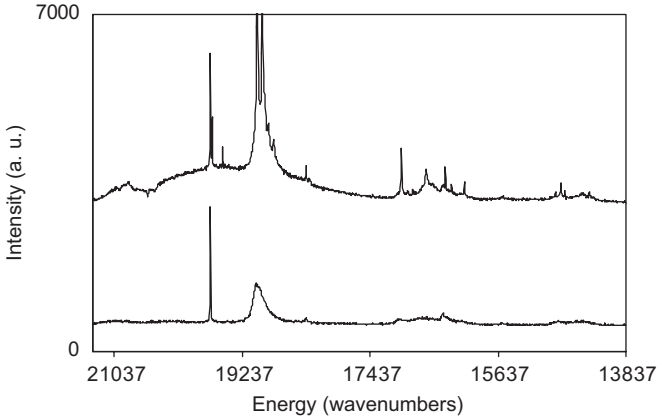

Fig. 7. Emission spectra of $Pr[Au(CN)_2]_3 \cdot 3H_2O$ at room temperature (bottom spectrum) and at liquid nitrogen temperature (top). The sharp band at 19,685 cm^{-1} is the Raman signal corresponding to the CN symmetric stretch. Assignments of the other bands are given in Table 4.

components. The observation of only three of the possible four Stark components is consistent with structural data where a D_{3h} site occupation is implied for the curium ion.

The emission spectrum of the $Cm[Au(CN)_2]_3 \cdot 3H_2O$ crystal is shown in Fig. 5(b). When compared with the Ag analog, the emission bands are observed at red-shifted positions. The most intense band, for example, is observed at 16,740 cm^{-1}; a red-shift by ~40 cm^{-1} when compared with the 16,780 cm^{-1} value observed for the Ag analog. The other bands are observed at 16,790 and 17,045 cm^{-1}.

In Fig. 6, of the lowest emission energy of the $^6D_{7/2} \rightarrow {}^8S_{7/2}$ transitions for the two compounds is compared with other selected solid-state curium compounds. For the curium halides, the emission band red-shifts on going from the chloride to the bromide to the iodide compounds [44–46]. The comparison indicates that the highest red-shifting corresponds to curium doped in borosilicate matrices [47]. The recently characterized iodate compound, $Cm(IO_3)_3$ [48], has an emission energy between the iodide and bromide compounds. In previous studies, an increased red-shift has been correlated with a decreased electronegativity of the halide in the emission spectra of CmX_3 ($X = F, Cl, Br, I$) [49]. The spectroscopic comparisons shown in Fig. 6 indicates that **1** has a value between that for the chloride and bromide compounds, whereas the Ag analog, **2**, has an emission band at the highest energy, 16,780 cm^{-1}.

For electronic transitions involving metal orbitals that participate directly in bonding, the relative decrease in inter-electronic repulsion in going from the free ion to compounds is known to cause a red-shift [50,51]. The relative decrease in percent of the inter-electronic repulsion is evaluated from the red-shifts and is correlated with the nephelauxetic effect [47,50–52]. However, unlike the transition metals, where *d* orbitals can participate directly in bonding, the cause for nephelauxetic effects in *f*-element spectroscopy is not well understood. Since the energies of *f* levels are primarily governed by spin–orbit coupling, it is not clear if the shift represents a weakening of the coupling. Experimentally, the red shift in *f–f* transitions has been correlated with the basicity of the coordinating ligand, where the largest shift is caused by the most basic ligand. According to Sinha's lanthanide nephelauxetic effect derived from spectroscopic data, O^{2-} is the most basic and F^- the least basic ligand [52]. Although red-shifts observed in 4*f*-lanthanide species are small (only a few hundred wavenumbers), shifts as high as 1100 cm^{-1} have been noted in actinide systems [49,53]. For example, the $^5L_6$ level of Am(III) shows a nephelauxetic shift of up to 5.6% within the halide series (F^- to I^- systems) [53]. Based on the spectroscopic comparisons described here, we infer that the electron donating ability of the $Au(CN)_2^-$ should be placed between the Cl^- and Br^- anions, whereas the $Ag(CN)_2^-$ anion will have the least among the series listed. The result is consistent with the well-established fact that gold is more prone to covalent interaction than silver.

3.4.2. *Pr[M(CN)$_2$]$_3$·3H$_2$O (M = Au, Ag)*

Spectroscopic properties of trivalent praseodymium ions have been extensively studied in various hosts and compounds because of rich emissions extending from the ultraviolet to the infrared. Optical properties of Pr^{3+} have great importance in functional photonic materials, optical fiber amplifiers, and wavelength converters [54,55]. Laser actions and scintillation properties have also been observed in some of the Pr^{3+} compounds [54,55]. Frequency up-conversion of orange light at 588 nm to blue light at 480 nm was observed in Pr-doped, fluorinated glasses [56].

The $Pr[M(CN)_2]_3 \cdot 3H_2O$ (M = Au, Ag) compounds are luminescent providing well-resolved spectra upon direct *f–f* excitation of the Pr^{3+} ion. The emission spectra of $Pr[Au(CN)_2]_3 \cdot 3H_2O$ are shown in Fig. 7. The lower spectrum shown in Fig. 7 was collected at room temperature. The emission from the *f*-excited levels of the Pr^{3+} ion is weak, presumably due to vibrational relaxation

and non-radiative de-excitation processes. The most dominant emission band at room temperature is the broad band observed at 18,980 cm^{-1} (~527 nm) that corresponds to the $^3P_0 \rightarrow {}^3H_5$ transition. Other weak transitions are also evident at 18,340, 16,380, and 14,600 cm^{-1}. The sharp band at 19,680 cm^{-1} corresponds to the ν_{CN} symmetric stretching Raman band.

Upon cooling the crystal in liquid N_2, a highly resolved emission profile is observed (top spectrum Fig. 7). The spectra were collected after excitation with the 457.6 nm line of an argon laser. The excitation wavelength matches the $^3H_4 \rightarrow {}^3P_1$ transition. Several emissions originating from more than one excited level ($^3P_0$, $^3P_1$, and $^1D_2$) are also observed. Although the most intense band in many Pr emission spectra [57–59] is located at ~15,500 cm^{-1} (~645 nm) and corresponds to the electric dipole ($\Delta J = 2$) $^3P_0 \rightarrow {}^3F_2$ transition, that is not the case for the spectra of both compounds reported here. The most intense band is observed in the 19,000–18,800 cm^{-1} region (526–532 nm) with several splittings corresponding to the $^3P_0 \rightarrow {}^3H_5$ transition. Four well-resolved bands are observed at 19,020, 18,950, 18,870, and 18,790 cm^{-1} with an overall separation of ~230 cm^{-1}.

Although a maximum of 11 bands are expected under a low-symmetry site occupation for the Pr^{3+} ion, the observance of only four well-resolved bands is consistent with the higher symmetry (D_{3h}) deduced from the X-ray data. In the 18,400–18,100 cm^{-1} (543–547 nm) region, three weak bands are resolved; the strongest of them located at 18,330 cm^{-1}. After comparing with literature data [54–59] we believe the transition in this region orginates from the $^3P_1$ excited level and corresponds to the $^3P_1 \rightarrow {}^3H_5$ transition. In the 17,000–16,800 cm^{-1} (588–594 nm) region an emission originating from the lower $^1D_2 \rightarrow {}^3H_4$ level is evident. The band at 17,000 cm^{-1} is the strongest in this region. A broader band is also apparent in the ~16,660 cm^{-1} region which is assignable to the $^3P_0 \rightarrow {}^3H_6$ transitions. The electric dipolar, $^3P_0 \rightarrow {}^3F_2$ transition, although weak, is also observed in the 16,400–16,100 cm^{-1} region (Table 4).

Details of the spectral transitions and the corresponding assignments are given in Table 4. A characteristic phenomenon of these complexes is that the electric dipole transition is less dominant when compared with the most intense $^3P_0 \rightarrow {}^3H_5$ transition, confirming that the Pr^{3+} ion is under a high symmetry site occupation. Further spectroscopic evidence for the high symmetry site occupation is the lack splitting in all of the emission transitions. It is interesting to note that the high, local site symmetry remains the same both in the X-ray and luminescence data; hence it can be concluded that the *f*-species site occupation is D_{3h}, as found from the X-ray data. In Fig. 8, is shown the liquid N_2 temperature data of the $Pr[Ag(CN)_2]_3 \cdot 3H_2O$ sample. Under direct *f–f* excitation both the silver and gold systems provide similar profiles, with only a slight shift in the emission energies. These shifts are indicated in Table 4. Based on the spectral similarities, we can conclude the Pr^{3+} ion in the $Pr[Ag(CN)_2]_3 \cdot 3H_2O$ has a high symmetry site occupation similar to what has been deduced for the $Pr[Au(CN)_2]_3 \cdot 3H_2O$ system.

Table 4
Emission bands and assignments for the Pr^{3+} ion the dicyanide complexes

$Pr[Au(CN)_2]_3$ (cm^{-1})	$Pr[Ag(CN)_2]_3$ (cm^{-1})	Assignment
19020	19000	$^3P_0 \rightarrow {}^3H_5$
18950	18960	
18870	18890	
18790	18820	
18410	18340	$^3P_1 \rightarrow {}^3H_5$
18330		
18290		
17000	17040	$^1D_2 \rightarrow {}^3H_4$
16900	16920	
16840		
16620	16730	$^3P_0 \rightarrow {}^3H_6$
16540	16680	
	16550	
16380	16400	$^3P_0 \rightarrow {}^3F_2$
16290	16300	
16120	16110	
	14830	$^1D_2 \rightarrow {}^3H_5$
	14770	
	14710	
	14480	$^3P_0 \rightarrow {}^3F_4$
	14370	
	14320	
	14270	

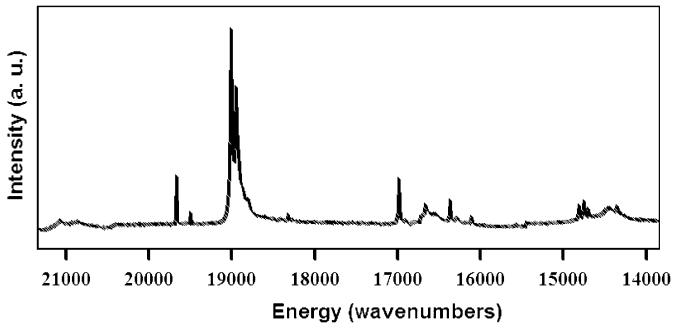

Fig. 8. Emission spectrum of $Pr[Ag(CN)_2]_3 \cdot 3H_2O$ at liquid N_2 temperature. The sharp band at 19,660 cm^{-1} is the Raman signal corresponding to the CN symmetric stretch.

4. Summary

The polymeric compounds between the man-made element, curium, and gold and silver dicyanides were prepared using the less-conventional hydrothermal synthetic procedure. The curium ion and the transition metals are interconnected through cyanide bridging. The structural and synthetic features of the $Cm[Au(CN)_2]_3 \cdot 3H_2O$ were also compared with the isostructural Pr compounds. All of

the compounds studied crystallize in the same hexagonal space group with only slight differences in their unit cell parameters. The coordination around the Cm or Pr consists of six CN^- groups coordinated through the N atoms resulting in a trigonal prismatic environment. Three oxygen atoms of coordinated water molecules complete the tricapped prismatic coordination environment providing a total coordination number of nine. The ν_{CN} stretching frequency of the compounds was used for comparison purposes. When compared with $KAg(CN)_2$ or $KAu(CN)_2$, the ν_{CN} stretching frequency in all the compounds blue-shifts due to bridging of the cyanide group. When compared with the silver systems, the ν_{CN} stretching frequency appears at higher energy in the gold dicyanide complexes. The luminescence properties of the compounds have been used to estimate the nephelauxetic effects where red-shifts on the emission bands have been observed.

Acknowledgments

Support for this work was provided by the Division of Chemical Sciences, Geosciences and Biosciences, OBES, USDOE, under Contract DE-AC05-00OR22725 with Oak Ridge National Laboratory, managed by UT-Battelle, LLC. The ^{248}Cm isotope used in these studies was supplied by the USDOE. Dr. Radu Custelcean and Dr. Bruce Moyer at ORNL are thanked for their generous allocation of X-ray diffractometer time. Support from the National Oceanic and Atmospheric Administration Educational Partnership Program (NOAA-EPP) award number NA06OAR4810187 to North Carolina A&T State University is also kindly acknowledged for part of the work conducted at NCAT State University. R.E.S. would like to thank Oak Ridge National Laboratory for the loan of an Enraf-Nonius CAD-4 diffractometer.

References

[1] C.E. Plecnik, L. Shengming, S.G. Shore, Acc. Chem. Res. 36 (2003) 499.
[2] B.-H. Xia, C.-M. Che, D.L. Phillips, K.-H. Leung, K.K. Cheung, Inorg. Chem. 41 (2002) 3866.
[3] K.R. Dunbar, R.A. Heintz, Prog. Inorg. Chem. 45 (1997) 283.
[4] M. Verdaguer, A. Bleuzen, V. Marvaud, J. Vaissermann, M. Seuleiman, C. Desplanches, A. Scuiller, C. Train, R. Garde, G. Gelly, C. Lomenech, I. Rosenman, P. Veillet, C. Cartier, F. Villain, Coord. Chem. Rev. 190 (1999) 1023.
[5] A. Figuerola, C. Diaz, M.S. El Fallah, J. Ribas, M. Maestro, J. Mahia, Chem. Commun. (2001) 1204.
[6] M. Ohba, H. Okawa, Coord. Chem. Rev. 198 (2000) 313.
[7] H. Vahrenkamp, A. Geib, G.N. Richardson, J. Chem. Soc., Dalton Trans. (1997) 3643.
[8] M.A. Omary, H.H. Patterson, J. Am. Chem. Soc. 120 (1998) 7696.
[9] M.A.-O. Rawashdeh, M.A. Omary, H.H. Patterson, J.P. Fackler, J. Am. Chem. Soc. 123 (2001) 11237.
[10] Z. Assefa, B.G. McBurnett, R.J. Staples, J.P. Fackler Jr., Inorg. Chem. 34 (1995) 4965.
[11] I.K. Chu, I.P.Y. Shek, K.W.M. Siu, W.-T. Wong, J.-L. Zuo, T.-C. Lau, New J. Chem. 24 (2000) 765.
[12] Z. Assefa, R.J. Staples, J.P. Fackler Jr., H.H. Patterson, G. Shankle, Acta Crystallogr. C 51 (1995) 2527.
[13] M.A. Rawashdeh-Omary, C.L. Larochelle, H.H. Patterson, Inorg. Chem. 39 (2000) 4527.
[14] J.M. Forward, J.P. Fackler, Z. Assefa, Optoelectronic properties of inorganic compounds, in: D.M. Roundhill, J.P. Fackler Jr. (Eds.), Plenum Press, New York, 1999, 195pp.
[15] Z. Assefa, G. Shankle, R. Reynolds, H.H. Patterson, Inorg. Chem. 33 (1994) 2187.
[16] R.J. Puddephatt, Coord. Chem. Rev. 216–217 (2001) 313–332.
[17] M.A. Omary, T.R. Webb, Z. Assefa, G.E. Shankle, H.H. Patterson, Inorg. Chem. 37 (1998) 1380.
[18] Z. Assefa, K. Kalachnikova, R.G. Haire, R.E. Sykora, J. Solid State Chem. 180 (2007) 3121.
[19] G.B. Andreev, M.Y. Antipin, A.M. Fedoseev, N.A. Budantseva, Kristallografiya 46 (3) (2001) 433–434.
[20] SADABS, Acta Crystallogr. A 51 (1995) 33.
[21] K. Harms, S. Wocadlo, XCAD4, University of Marburg, Germany, 1995.
[22] G.M. Sheldrick, SHELTXL PC, Version 5.0, An Integrated System for Solving, Refining, and Displaying Crystal Structures from Diffraction Data, Siemens Analytical X-ray Instruments, Inc., Madison, WI, 1994.
[23] A.J.C. Wilson, International Tables for Crystallography, Vol. C, Mathematical, Physical and Chemical Tables, Kluwer Academic Publishers, Boston, 1992.
[24] J.C.F. Colis, C. Larochelle, R. Staples, R. Herbst-Irmer, H.H. Patterson, Dalton Trans. (2005) 675.
[25] J.C.F. Colis, R.J. Staples, C. Tripp, D. Labrecque, H.H. Patterson, J. Phys. Chem. B 109 (2005) 102.
[26] S.J. Hibble, S.G. Eversfield, A.R. Cowley, A.M. Chippindale, Angew. Chem. Int. Ed. 43 (2004) 628.
[27] T. Pretsch, I. Brüdgam, H. Hartl, Z. Anorg. Allg. Chem. 630 (2004) 353.
[28] P.A. Tanner, X. Zhou, W.-T. Wong, C. Kratzer, H. Yersin, J. Phys. Chem. B 109 (2005) 13083.
[29] K. Kalachnikova, Z. Assefa, R.E. Sykora, Acta Crystallogr. E 63 (2007) i162.
[30] J.N. Stevenson, J.R. Peterson, J. Less-Common Met. 66 (2) (1979) 201.
[31] R.E. Sykora, Z. Assefa, R.G. Haire, T.E. Albrecht-Schmitt, J. Solid State Chem. 177 (2004) 4413.
[32] J.R. Peterson, J.H. Burns, J. Inorg. Nucl. Chem. 35 (1973) 1525.
[33] P. Lindqvist-Reis, C. Apostolidis, J. Rebizant, A. Morgenstern, R. Klenze, O. Walter, T. Fanghänel, R.G. Haire, Angew. Chem. 119 (2007) 937.
[34] S. Skanthakumar, M.R. Antonio, R.E. Wilson, L. Soderholm, Inorg. Chem. 46 (2007) 3485.
[35] L. Soderholm, S. Skanthakumar, C.W. Williams, Phys. Rev. B 60 (1999) 4302.
[36] L.R. Morss, J.W. Richardson Jr., C.W. Williams, G.H. Lander, A.C. Lawson, N.M. Edelstein, G.V. Shalimoff, J. Less-Common Met. 156 (1989) 273.
[37] P. Pyykko, Angew. Chem. Int. Ed. 43 (2004) 4412.
[38] P. Pyykko, Inorg. Chim. Acta 358 (2005) 4113.
[39] A. Bayler, A. Schier, G.A. Bowmaker, H. Schmidbauer, J. Am. Chem. Soc. 118 (1996) 7006.
[40] Z. Assefa, H.H. Patterson, Inorg. Chem. 33 (1994) 6194.
[41] I. Muga, J.M.G. Zorrilla, P. Vitoria, P. Roman, L. Lezama, J.I. Beitia, Eur. J. Inorg. Chem. (2004) 1886.
[42] M.J. Katz, P.M. Aguiar, R.J. Batchelor, A.A. Bokov, Z.-G. Ye, S. Kroeker, D.B. Leznoff, J. Am. Chem. Soc. 128 (2006) 3669.
[43] E.C.-C. Cheng, K.-H. Leung, V.M. Miskowski, V.W.-W. Yam, D.L. Phillips, Inorg. Chem. 39 (2000) 3690.
[44] N.A. Stump, G.M. Murray, G.D. Del-Cul, R.G. Haire, J.R. Peterson, Radiochim. Acta 61 (1993) 129.
[45] G.M. Murray, G.D. Del Cul, G.M. Begun, R.G. Haire, J.P. Young, J.R. Peterson, Chem. Phys. Lett. 168 (1990) 473.

[46] Y.A. Barbanel, G.P. Chudnovskaya, Y.I. Gavrish, R.B. Dushin, V.V. Kolin, V.P. Kotlin, Radioanal. Nucl. Chem. 143 (1990) 113.
[47] Z. Assefa, R.G. Haire, N.A. Stump, Mat. Res. Soc. Symp. Proc. 556 (1999) 359.
[48] R.E. Sykora, Z. Assefa, R.G. Haire, T.E. Albrecht-Schmitt, Inorg. Chem. 44 (2005) 5667.
[49] Y.A. Barbanel, V.R. Klokman, V.P. Kotlin, V.V. Kolin, Y.I. Gavrish, A.N. Smirnov, Radiokhimiya 24 (1982) 580.
[50] M. Williams, R.T. Brundage, Phys. Rev. B 45 (1992) 4561.
[51] M. Shiloh, M. Givon, Y. Marcus, J. Inorg. Nucl. Chem. 31 (1969) 1807.
[52] S.P. Sinha, Complexes of the Rare Earths, Pergamon Press, Oxford, 1966, p. 106.
[53] Y.A. Barbanel, Radiochemistry 38 (1996) 27.
[54] Y. Yokokawa, H. Inokuma, Y. Ohki, H. Nishikawa, Y. Hama, J. Appl. Phys. 77 (1995) 4013.
[55] L.R. Moorthy, T.S. Rao, K. Janardhanam, A. Radhapathy, J. Alloys Compd. 298 (2000) 59.
[56] D.R. MacFarlane, Ceram. Int. 22 (1996) 535.
[57] K. Bris, C. Reber, J. Alloys Comp. 424 (2006) 237.
[58] K. Horchani, J.C. Gacon, M. Ferid, M. T-Ayedi, O. Krachni, G.K. Liu, Opt. Mater. 24 (2003) 169.
[59] J. Legendziewicz, J. Cybinska, G. Meyer, Opt. Mater. 24 (2003) 197.